Nonlinear Processes in Geophysics (1998) 5: 167–179

Nonlinear Processes in Geophysics

Dynamical implications of prescribing part of a coupled system: Results from a low-order model

A. T. Wittenberg[1] and J. L. Anderson[2]

[1]Program in Atmospheric and Oceanic Science, Princeton University, Princeton, NJ 08542, USA
[2]GFDL/NOAA, Princeton, NJ 08542, USA

Received: 26 November 1998 – Accepted: 13 March 1999

Abstract. It is a common procedure in climate modeling to specify dynamical system components from an external source; a prominent example is the forcing of an atmospheric model with observed sea surface temperatures. In this paper, we examine the dynamics of such forced models using a simple prototype climate system. A particular fully-coupled run of the model is designated the "true" solution, and an ensemble of perturbed initial states is generated by adding small errors to the "true" initial state. The perturbed ensemble is then integrated for the same period as the true solution, using both the fully-coupled model and a model in which the ocean is prescribed exactly from the true solution at every time step. Although the prescribed forcing is error-free, the forced-atmosphere ensemble is shown to converge to spurious solutions. Statistical tests show that neither the time-mean state nor the variability of the forced ensemble is consistent with the fully-coupled system. A stability analysis reveals the source of the inconsistency, and suggests that such behavior may be a more general feature of models with prescribed subsystems. Possible implications for model validation and predictability are discussed.

1 Introduction

Although the ocean and atmosphere comprise a unified fluid system, it is often convenient to separate them conceptually to simplify model analysis and development. It is a common practice, for example, to force an atmospheric model with observed sea surface temperatures (SSTs). The Atmospheric Model Intercomparison Project (AMIP; Gates, 1992) used this paradigm to characterize various atmosphere models, and the approach has been used extensively in dynamical studies (Lau, 1985; Latif et al., 1990; Lau and Nath, 1994; Graham et al., 1994; Ward and Navarra, 1997), assessments of predictability (Miller and Roads, 1990; Stern and Miyakoda, 1995; Chen and Van den Dool, 1997) and investigations of forced climate variability (Kang and Lau, 1986; Harzallah and Sadourny, 1995; Rowell et al., 1995; Kumar et al., 1996). A related technique, known as "two-tiered" forecasting, uses SSTs predicted by a simplified coupled model to force an atmospheric GCM forecast (Bengtsson et al., 1993; Barnett, 1995; Battisti and Sarachik, 1995; Livezey et al., 1996). This "forced-atmosphere" approach is designed to constrain the atmospheric model to a realistic time-mean state, which can be essential for proper simulation of the variability (McCreary and Anderson, 1991; Philander, 1992; Latif et al., 1997).

Yet it is not clear to what extent a model with prescribed components must emulate a fully-coupled system. Roebber et al. (1997) showed that forcing with time-averaged SSTs, instead of instantaneous SSTs, could alter the variability and predictability of a simple atmospheric model. Beyond the question of the fidelity of the prescribed forcing, there is another, more fundamental issue. Specifying part of a coupled system essentially changes its dynamics, by preventing feedbacks from modifying the imposed forcing. This difference could give rise to dynamical inconsistencies between forced and fully-coupled simulations.

Recent work (Gallimore, 1995; Bladé, 1997; Saravanan and McWilliams, 1997, 1998; Barsugli and Battisti, 1998) provides an example of a forced-model inconsistency in mid-latitude ocean-atmosphere systems. Consider a cold surface air temperature (SAT) anomaly overlying a warm SST anomaly. In nature, the surface air is free to interact with the ocean surface through heat fluxes. As the SAT warms towards the SST, the SST also cools towards the SAT, so that the effective damping of the SAT anomaly decreases with time. When the SST is specified as in an AMIP-type model, however, the ocean can no longer respond to SAT anomalies. As a result, air-sea heat fluxes become unrealistically large and SAT anomalies are too strongly damped. Thus in this case a model with specified SSTs will overestimate the true variance of the heat fluxes, and underestimate the true variance of surface air temperatures.

Other studies have demonstrated that specifying part of

Correspondence to: A. T. Wittenberg

a strongly-coupled system can bias the attribution of cause and effect in the system. Saravanan and McWilliams (1998) found that a model with specified SSTs failed to reproduce the air-sea temporal covariances of a coupled model: SAT led SST in the latter, but not in the former. In the study of Saravanan (1998), an AMIP model portrayed the atmosphere's effect as primarily one of *damping* SST anomalies. The coupled model, however, revealed that atmospheric variability was actually *forcing* these SST anomalies.

Such studies could have important implications for imposed-forcing paradigms such as AMIP. Because the climate system's time-mean state and variability are both determined by coupled feedbacks, eliminating these feedbacks might alter both the climate and the variability of a forced model. Tuning an atmosphere or ocean GCM in this context might then predispose it to failure as a component of a fully-coupled system.

This paper explores the dynamical implications of prescribing system components from an external source. Section 2 describes a prototype coupled system. Section 3 shows how the variability of this system's "atmospheric" component changes when its "ocean" component is prescribed rather than predicted, and Section 4 explains why the forced and coupled systems evolve differently. Section 5 reveals some differences in the spread-skill relationship between forced and coupled ensembles. Section 6 concludes with a discussion of how the low-order model results might apply to GCMs.

2 A prototype coupled system

Consider as a prototype "climate system" the five-variable model of Goswami et al. (1993):

$$\frac{dx}{dt} = -(y^2+z^2) - ax + af \tag{1}$$

$$\frac{dy}{dt} = xy - cy + g - bxz + \alpha p \tag{2}$$

$$\frac{dz}{dt} = xz - cz + bxy + \alpha q \tag{3}$$

$$\frac{dp}{dt} = -\omega q - \beta y \tag{4}$$

$$\frac{dq}{dt} = \omega p - \beta z \tag{5}$$

Details of the model are given in the appendix, and trajectories of the model atmosphere and ocean are shown in Fig. 1. For our purposes the coupled system (1)–(5) will describe the evolution of an idealized "atmosphere" $\psi^A(t) = (x, y, z)^T$ and "ocean" $\psi^S(t) = (p, q)^T$. Throughout this paper, ^{T} will denote a matrix transpose, while ^{A} and ^{S} will indicate vectors which contain only "atmosphere" variables (x, y, z) or "sea" variables (p, q). This low-order model is clearly too simple to describe the detailed *physics* of a realistic climate system. However, the model will prove to be a useful conceptual tool. It will facilitate an investigation of some common *dynamical* features of models forced with prescribed components, and will provide analogues for the behavior of more complicated systems of this type. In certain ways the model imitates a coupled GCM: it is forced, dissipative, and chaotic; the atmosphere is more rapidly-evolving and nonlinear than the ocean; and air-sea interactions produce variability with multiple time scales in both components.

Very long integrations indicate that trajectories $\psi(t) = (x, y, z, p, q)^T$ of the coupled model are bounded, and depend sensitively on the initial state $\psi(0)$. The numerical model is found to be aperiodic for at least 10^9 years when integrated using 64-bit floating point precision. Since the coupled model is dissipative, volumes in its five-dimensional phase space shrink exponentially in time; thus an initial cloud of phase space points eventually gets stretched thin along the model's attractor. The attractor is *chaotic* in that the model evolution depends sensitively on its initial state, and *strange* in that trajectories appear to skip around randomly. Since this finite-dimensional bounded system must eventually approach some previous state arbitrarily closely, the attractor is *ergodic* on long time scales. The coupled model atmosphere has an ergodic time scale on the order of decades. The coupled model ocean, with its low natural frequency ω, has an ergodic time scale on the order of millennia.

3 Variability of a prototype forced model

3.1 Forced-atmosphere experiments

A forced-atmosphere experiment schematic is given in Fig. 2. To attain steady statistics, the coupled model is integrated for 500 years prior to the period of analysis. Following the coupled spinup, the initial state $\psi(0)$ is integrated for 2000 years via the coupled model to produce the *true solution* $\psi(t)$, which consists of the "true atmosphere" solution $\psi^A(t)$ and the "true sea" solution $\psi^S(t)$. Next, an ensemble of N perturbed atmospheres $\psi_j^A(0), j = 1, \ldots, N$ is generated at the initial time by adding random errors to the true initial atmosphere $\psi^A(0)$; the initial atmospheric error vectors $\delta_j^A(0) = \psi_j^A(0) - \psi^A(0)$ are selected at random from a Gaussian distribution with standard deviation ε for each model variable (x, y, z). The perturbed states are then integrated for the same period as the true solution, first via the coupled model to produce *perturbed coupled solutions* $\psi_{C(j)}$, and then via a *forced-atmosphere (AMIP)* model to produce *perturbed forced-atmosphere solutions* $\psi_{F(j)}^A$. In the forced-atmosphere model, ψ_F^A is governed by (1)–(3) only, with the ocean prescribed exactly from the true sea ψ^S at every time step. By design, the forced model reproduces the true solution exactly if integrated forward from the true initial state $\psi(0)$ (see appendix).

Fig. 3 shows a segment from an experiment with $N = 9$, starting 65 years after initial perturbations with $\varepsilon = 0.01$. The forced ensemble is generally more compact than the coupled ensemble, especially when the forced ensemble most resembles the true solution (years 67 and 68). Often the forced

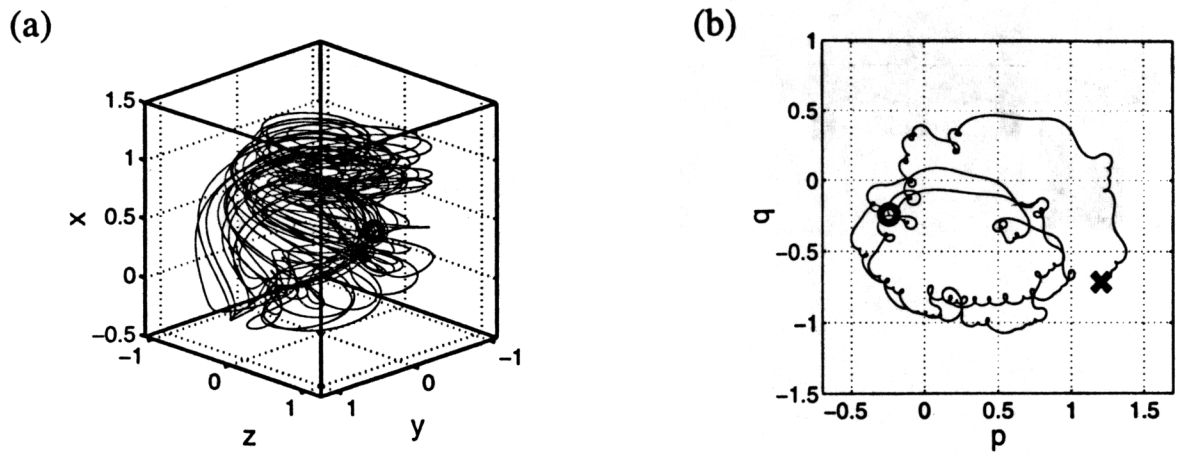

Fig. 1. Eight-year trajectories of the prototype coupled system for (a) atmospheric variables $\psi^A(t) = (x, y, z)^T$ and (b) oceanic variables $\psi^S(t) = (p, q)^T$. The initial and final states are marked with a cross and a circle, respectively. The system is spun up by integrating for 500 years prior to the period shown.

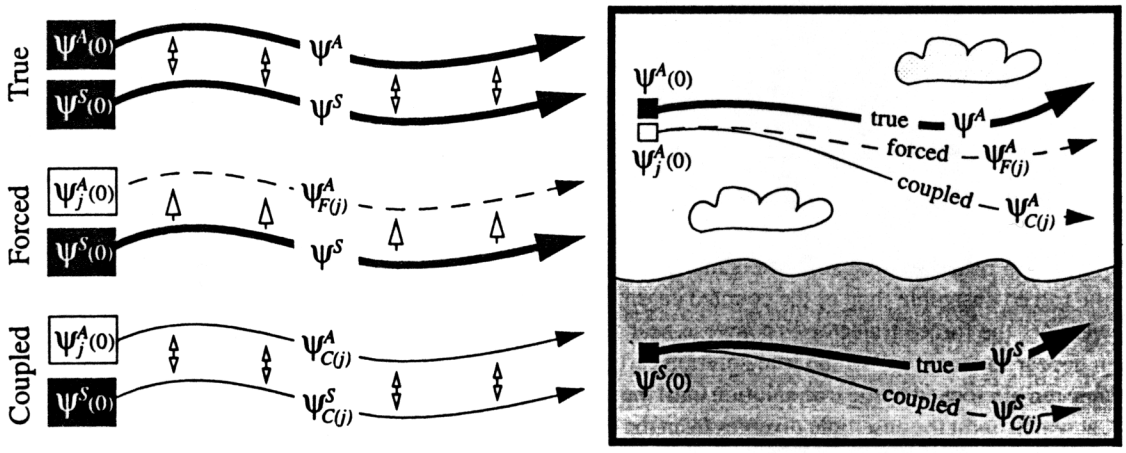

Fig. 2. Two representations of the integration scheme for a forced-atmosphere (AMIP) experiment. Dark boxes represent the "true" initial state $\psi(0) = (\psi^A(0), \psi^S(0))$, which is integrated forward in time via the coupled model to produce the "true solution" $\psi(t)$ (thick lines). Open boxes denote a member $\psi_j^A(0)$ of an ensemble of perturbed atmospheric initial states. Each $\psi_j^A(0)$ is integrated via the forced-atmosphere model to produce a perturbed forced-atmosphere trajectory $\psi_{F(j)}^A(t)$ (dashed lines), and via the coupled model to produce a perturbed coupled trajectory $\psi_{C(j)}^A(t)$ (thin solid lines).

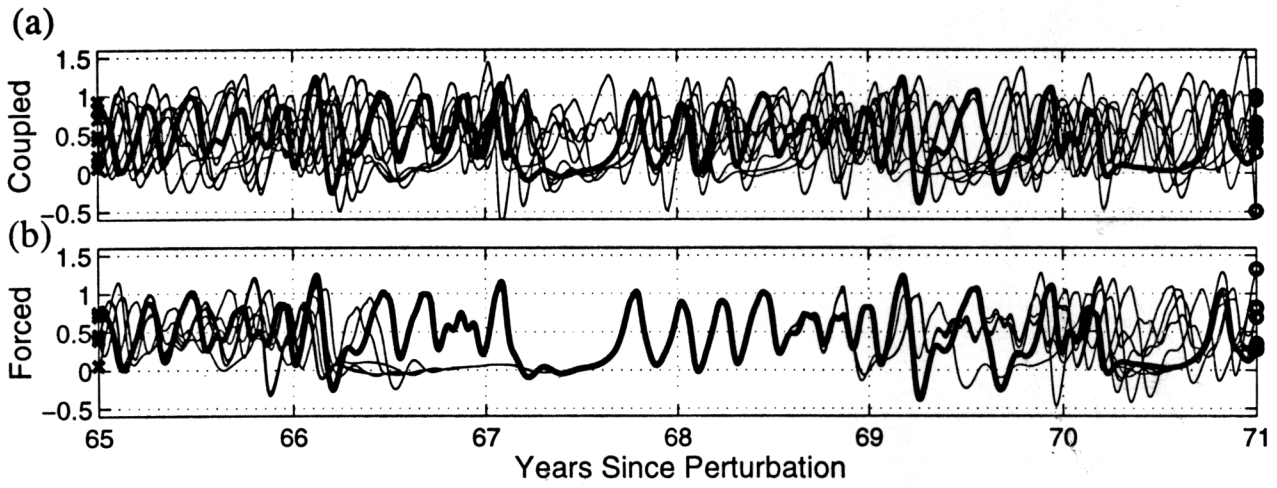

Fig. 3. Time series of the atmospheric variable x for (a) the perturbed coupled ensemble and (b) the perturbed forced ensemble. Each ensemble has 9 members. The true solution is superposed with a thick line. Years 65 through 70 after the initial perturbation are shown.

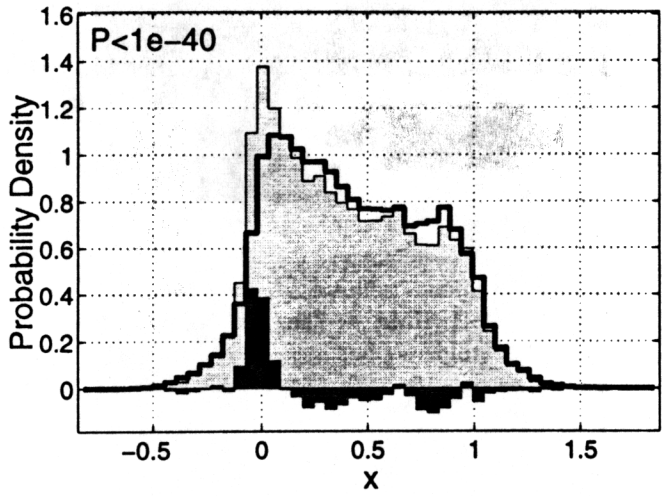

Fig. 4. Probability densities for the atmospheric variable x in the coupled model (dark line) and in the forced model (light shading). The difference between these densities is also shown (dark shading). The 9 members of each ensemble were sampled every 100 days for 2000 years, yielding 65 754 samples each of the coupled and forced attractors. P denotes the KS significance for the comparison of coupled and forced distributions; $P \ll 1$ confirms the inconsistency of the distributions for this model variable.

ensemble is compact, but not constrained to the true solution (year 66). As a result the true solution is more often an outlier of the forced ensemble than of the coupled ensemble.

During year 66, the forced trajectories converge near $x = 0$, and then appear to "lock on" to the true solution early in year 67. They remain locked to the true solution until the end of year 68, at which point the ensemble diverges from the true solution but remains compact. At the start of year 69, the ensemble splits into two compact groups. By the middle of year 70, four of the nine forced members have again locked to the true solution, while the others have spread apart. Although the true solution often tarries near $x = 0$, as in years 67 and 70, it never remains in this vicinity longer than a few months. The forced solutions, however, often linger near $x = 0$ for extended periods (e.g., years 66–67). This is a first hint that the forced climatology may not emulate the "true" coupled climatology.

3.2 Spatial distributions

Fig. 4 compares binned probability densities of the variable x for a 2000-year experiment with $N = 9$. Snapshots of the perturbed coupled and forced ensembles were taken every 100 days between years 20 and 2020 after perturbation, giving 65 754 samples each of the coupled and forced attractors. The histograms show that forced trajectories spend more time near $x = 0$ than do coupled trajectories.

The *Kolmogorov-Smirnov (KS) test* (Press et al., 1992) is used to estimate the significance of differences between spatial distributions of the forced and coupled ensembles. The test defines a statistic

$$D \equiv \max |S_{N_1}(x) - S_{N_2}(x)|$$

which is the maximum absolute difference between two cumulative distributions. The S_{N_i} are the cumulative distribution functions of the two data sets; they give the fraction of the N_i data points which have values smaller than x. In the case of the *null hypothesis* that the data sets were drawn from the same distribution, one can calculate the probability P that D could be as large as observed. If the null hypothesis is correct, independent realizations of P will be uniformly distributed on the interval $(0, 1]$. The smaller the probability P, the less likely the samples were drawn from the same distribution. Because the coupled model is chaotic, spinning up the model from different initial states eventually yields independent solutions. Since the true and perturbed coupled solutions are realizations of the same coupled model, independent experiments should yield values of P uniformly distributed on $(0, 1]$. Thus if we perform a large number of experiments, we expect an average significance $\bar{P} = 0.5$ for the comparison of the true and perturbed coupled solutions.

Table 1 lists the KS significances for each variable and for various model intercomparisons, averaged over ten experiments (ten realizations of P). The values in row 1 are close to 0.5, consistent with the assumption that the coupled system is ergodic on these time scales. However, the very low significances in rows 2 and 3 confirm that the perturbed forced solutions do not have the same spatial distribution as the true or perturbed coupled solutions. This was apparent in Fig. 4, which showed that forced solutions spend more time near $x = 0$ than do coupled solutions. Apparently the forced model lacks feedback mechanisms which pull the coupled model away from $x = 0$. These mechanisms can operate in the forced model only when the atmosphere is close to the true solution, so that the prescribed ocean provides forcing consistent with the coupled system.

3.3 Temporal distributions

As we have seen, the forced ensemble is often too compact to contain the true solution within its spread, as in years 66 and 69 of Fig. 3. This suggests that the forced model may be temporally inconsistent with the true coupled system. We investigate this possibility by analyzing the rank of the true solution within the forced and coupled ensembles.

At each time t, an N-ensemble and the true solution together provide $N + 1$ values for the variable x. If we sort these $N + 1$ values in ascending order, the position of the

Table 1. Average, over 10 experiments, of the Kolmogorov-Smirnov significances for intercomparisons of spatial distributions of the true solution, the coupled ensemble, and the forced ensemble. Subscripts on $\bar{P}$ denote the model variable being compared. $\bar{P} \ll O(0.5)$ implies that the spatial distributions are inconsistent.

Comparison	$\bar{P}_x$	$\bar{P}_y$	$\bar{P}_z$	$\bar{P}_p$	$\bar{P}_q$
coupled & true	.54	.58	.41	.51	.36
forced & true	10^{-8}	10^{-6}	10^{-3}	*	*
coupled & forced	10^{-40}	10^{-38}	10^{-21}	*	*

* The ocean is prescribed exactly from the truth in the forced model.

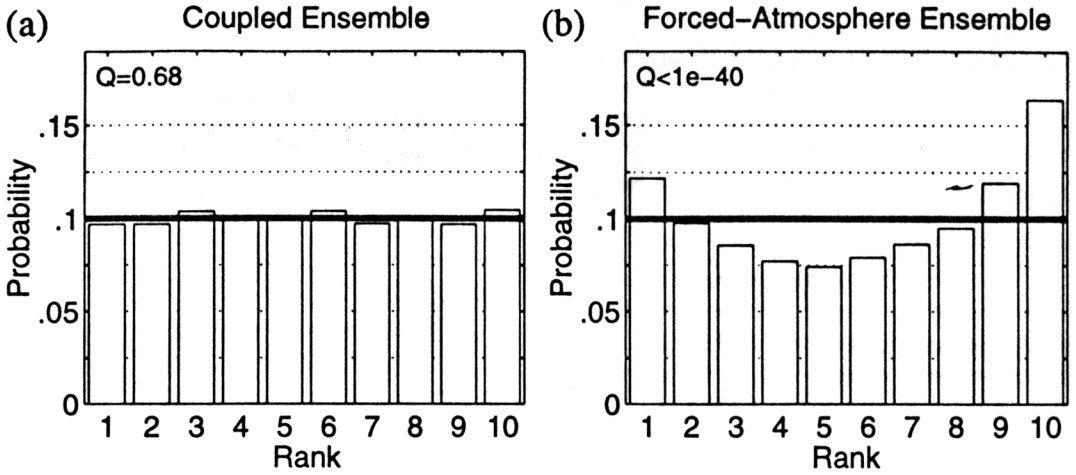

Fig. 5. Rank probabilities Γ_x of the true solution for x within (a) the coupled 9-ensemble and (b) the forced 9-ensemble. Trajectories were sampled every 100 days for 2000 years, giving 7306 realizations of Γ_x. Q denotes the chi-square significance of uniformity; $Q \ll 1$ implies inconsistency of the true solution and ensemble for this model variable.

true value of $x(t)$ defines a *rank statistic* Γ_x. By definition, $\Gamma_x = 1$ when the true value of x is smaller than those of all the ensemble members, and $\Gamma_x = N+1$ when the true value of x is larger than those of all the ensemble members. (In the event that the true x is exactly equal to one or more ensemble members, the "tie" is resolved by assigning a random Γ_x from the set of possible ranks; e.g. if the true x is tied for third with two ensemble members, Γ_x is chosen at random from the set $3, 4, 5$. At 64-bit precision, this almost never occurs.) The rank statistics Γ_y, Γ_z, Γ_p, and Γ_q are similarly defined for the model variables y, z, p, and q.

Since the atmospheric attractor is ergodic on decadal time scales, infrequent snapshots resemble "random" samples of the attractor. If the true solution and perturbed samples of x are selected in independent, random trials from identical distributions, then they should have no preferred order when sorted according to rank, and Γ should assume each value from 1 to $N+1$ with uniform probability $(N+1)^{-1}$. If the rank statistics are observed to be significantly nonuniform, then the ensemble solutions must be temporally inconsistent with the true solution (Anderson, 1996).

Fig. 5 gives histograms of Γ_x for coupled and forced ensembles with $N = 9$. Snapshots of the true solution, the coupled ensemble and the forced ensemble were taken every 100 days between years 20 and 2020, giving a total of 7306 realizations of Γ_x. In Fig. 5a the rank statistics are nearly uniform, consistent with the assumption that the coupled system is ergodic on these time scales. In Fig. 5b, however, the rank statistics are skewed toward extreme values, suggesting that the true solution is too often near the outer edges of the forced ensemble for the true solution and forced solutions to be consistent. The true solution also tends to lie toward greater values of x than does the forced ensemble, confirming the spatial bias noted in Fig. 4.

The significance of these results is estimated using the *chi-square test* (Press et al., 1992). We assign a statistic χ^2 to the non-uniformity of the Γ-histogram, with larger values of χ^2 indicating less uniformity:

$$\chi^2 \equiv \sum_{\Gamma=1}^{N} \frac{(n_\Gamma - n_{\text{avg}})^2}{n_{\text{avg}}}$$

where n_Γ is the number of hits to the rank Γ, and $n_{\text{avg}} = (7306 \text{ hits})/(N+1)$ is the average number of hits per rank. In the case of the null hypothesis that the ranks arise from a uniform distribution, one can calculate the probability Q that χ^2 could be as large as observed. If the null hypothesis is correct, independent realizations of Q will be uniformly distributed on the interval $(0, 1]$. The smaller the probability Q, the less likely the Γ were drawn from a uniform distribution, and the less likely the two systems sampled are temporally consistent. Since the true and perturbed coupled solutions are realizations of the same coupled model, independent experiments should yield values of Q uniformly distributed on $(0, 1]$ if the integrations are long enough for the ergodic assumption to hold. Thus if we perform a large number of experiments, we expect an average significance $\bar{Q} = 0.5$ for the comparison of the true and perturbed coupled solutions.

Table 2 lists the significances of uniformity of ranks for each model variable, averaged over 10 experiments (10 realizations of Q). The values in row 1 are close to 0.5, consistent with the assumption that the coupled model is ergodic on these time scales. However, the very low significance values in rows 2 and 3 confirm that the perturbed forced solutions

Table 2. Average, over 10 experiments, of chi-square significances of uniformity of rank statistics, for the coupled and forced ensembles. Subscripts on $\bar{Q}$ denote the model variable being compared. $\bar{Q} \ll O(0.5)$ implies that the true solution and the ensemble are temporally inconsistent.

Ensemble	$\bar{Q}_x$	$\bar{Q}_y$	$\bar{Q}_z$	$\bar{Q}_p$	$\bar{Q}_q$
Coupled	.45	.47	.46	.42	.42
Forced	10^{-40}	10^{-40}	10^{-40}	*	*

* The ocean is prescribed exactly from the truth in the forced model.

do not have the same temporal distribution as the true or perturbed coupled solutions. This lends confidence to the result pictured in Fig. 5: the true atmosphere is much more often an outlier of the forced ensemble than of the coupled ensemble.

This section has shown that the statistics of forced variability can be significantly different from those of coupled variability, even when the prescribed forcing is error-free and perfectly compatible with the coupled model. When feedbacks are absent, as in the forced model, the ensemble atmospheres are inconsistent with the true solution *even though the oceans are the true solution exactly.* In this case, it appears that accurate statistics of variability in the prototype model depend more on integrated air-sea feedbacks than on the instantaneous accuracy of the ocean state.

Given the simplicity of the prototype model, it is certainly feasible to consider ensemble sizes much larger than $N = 9$. However, this is not required for delineating the model probability density, since the runs are long and the model is ergodic. Nor is it required for the rank statistics, whose chi-square significance is a function of the number of hits to each rank; for a fixed number of snapshots, the number of hits to each rank (and therefore the confidence) *decreases* as the ensemble size increases. Although increasing N would increase the rank-resolution of the histograms in Fig. 5, $N = 9$ appears sufficient to illustrate our main points — that the true x-value tends to lie outside the forced ensemble, and that the forced ensemble is skewed toward lower x-values than the true solution. Using only nine members also demonstrates that if the runs are long enough, valuable information about a system can be obtained using only a small ensemble.

4 Theory

4.1 Formulation of the problem

Consider a dynamical system of the form

$$\frac{d\psi}{dt} = \mathbf{C}_\psi \psi + \mathcal{B}(t) \tag{6}$$

where $\mathbf{C}_\psi$ is an *autonomous* (not explicitly time-dependent) operator evaluated at the state vector ψ, and $\mathcal{B}(t)$ represents a non-autonomous forcing evaluated at time t. We shall use subscripts on non-constant operators to denote where they are evaluated in space. Now suppose that (6) represents an ocean-atmosphere system with linear coupling. Then $\mathbf{C}_\psi$ consists of an *uncoupled autonomous* (UA) part and an air-sea interaction part:

$$\begin{aligned} \frac{d\psi}{dt} &= (\mathbf{U}_\psi + \mathbf{K})\,\psi + \mathcal{B}(t) \qquad (7)\\ \mathbf{U}_\psi &\equiv \begin{pmatrix} \mathbf{A}_{\psi^A} & 0 \\ 0 & \mathbf{S}_{\psi^S} \end{pmatrix} \\ \mathbf{K} &\equiv \begin{pmatrix} 0 & \mathbf{K}^{S\to A} \\ \mathbf{K}^{A\to S} & 0 \end{pmatrix} \end{aligned}$$

where $\mathbf{U}_\psi$ contains the uncoupled "air" and "sea" operators, and $\mathbf{K}$ contains the air-sea interaction matrices. A forced model, as defined in Section 2, is simply (7) with air-sea interactions prescribed from the true solution:

$$\frac{d\psi_F}{dt} = \mathbf{U}_{\psi_F}\psi_F + \mathbf{K}\psi + \mathcal{B}(t) \tag{8}$$

The vector ψ_F here represents the state of two forced models: a forced-atmosphere ("AMIP") model and a complementary forced-ocean ("OMIP") model. $\mathbf{U}_{\psi_F}$ is the UA operator evaluated at ψ_F.

The *difference vector* between two states is given by

$$\delta_{m,n} \equiv \psi_m - \psi_n \tag{9}$$

The second subscript is omitted when $\psi_n = \psi$, so that δ_m denotes an *error vector* which represents a difference from the true solution. The subscripts m and n in (9) are place holders for "$C(j)$" or "$F(j)$", which denote the j^{th} member of the coupled or forced ensemble, respectively. The "(j)" usually will be omitted for readability.

If the vector function $\mathbf{U}_\psi\psi$ defined in (7) is everywhere analytic, (8) can be expanded about the true solution in powers of the "forced error" $\delta_F = \psi_F - \psi$:

$$\frac{d(\psi + \delta_F)}{dt} = \mathbf{U}_\psi\psi + \mathbf{U}'_\psi\delta_F + O(\delta_F^2) + \mathbf{K}\psi + \mathcal{B}(t) \tag{10}$$

where $O(\delta_F^2)$ denotes nonlinear error terms obtained from the multiple power series expansion of $\mathbf{U}_{\psi_F}\psi_F$. The *UA Jacobian* $\mathbf{U}'_\psi$ is the Jacobian of the vector function $\mathbf{U}_{\psi_F}\psi_F$, evaluated at the true solution ψ. This matrix gives the instantaneous linear tendency of any small perturbation η relative to the trajectory ψ:

$$\begin{aligned} \frac{d\eta}{dt} &= \mathbf{U}'_\psi\eta \qquad (11)\\ \mathbf{U}'_\psi &= \begin{pmatrix} \mathbf{A}'_{\psi^A} & 0 \\ 0 & \mathbf{S}'_{\psi^S} \end{pmatrix} \end{aligned}$$

Eigenvalues of $\mathbf{U}'_\psi$ with positive real parts correspond to "UA-divergent" directions, along which the projection of η grows. Eigenvalues with negative real parts correspond to "UA-convergent" directions, along which the projection of η shrinks. Eigenvalues of zero correspond to "UA-neutral" directions along which the projection of η is constant.

Subtracting (7) from (10) gives

$$\frac{d\delta_F}{dt} = \mathbf{U}'_\psi\delta_F + O(\delta_F^2) \tag{12}$$

which simultaneously describes the evolution of forced-atmosphere and forced-ocean errors. It is now clear that the forced errors evolve in a completely uncoupled and autonomous manner. When the $O(\delta_F^2)$ terms can be ignored relative to $\mathbf{U}'_\psi\delta_F$ in (12), then δ_F will evolve just like η in (11); forced errors will increase along UA-divergent directions, decrease along UA-convergent directions, and remain constant along UA-neutral directions.

4.2 Analysis of the prototype system

For the prototype system (1)-(5), we have

$$\mathbf{A}_{\psi^A} = \begin{pmatrix} -a & -y & -z \\ y & -c & -bx \\ z & bx & -c \end{pmatrix}$$

$$\mathbf{A}'_{\psi^A} = \begin{pmatrix} -a & -2y & -2z \\ y-bz & x-c & -bx \\ z+by & bx & x-c \end{pmatrix}$$

$$\mathbf{S} = \begin{pmatrix} 0 & -\omega \\ \omega & 0 \end{pmatrix} = \mathbf{S}'_{\psi^S}$$

$$\mathbf{K}^{A\to S} = \begin{pmatrix} 0 & -\beta & 0 \\ 0 & 0 & -\beta \end{pmatrix}$$

$$\mathbf{K}^{S\to A} = \begin{pmatrix} 0 & 0 \\ \alpha & 0 \\ 0 & \alpha \end{pmatrix}$$

$$\mathcal{B}(t) = (af(t), g, 0, 0, 0)^T$$

Since the coupled model (1)–(5) has only quadratic nonlinearities, the expansion in (12) terminates at second order:

$$\frac{d\delta_F}{dt} = \left(\mathbf{U}'_\psi + \mathbf{N}_{\delta_F}\right)\delta_F \tag{13}$$

$$\mathbf{N}_{\delta_F} = \begin{pmatrix} \hat{\mathbf{A}}_{\delta_F^A} & 0 \\ 0 & 0 \end{pmatrix}$$

where for the present case $\hat{\mathbf{A}}_{\delta_F^A}$ is simply the UA atmosphere operator with damping removed (i.e., $\mathbf{A}_{\psi^A}$ with $a = c = 0$), evaluated at δ_F^A. Separating (13) into air and sea components, we have

$$\frac{d\delta_F^A}{dt} = \left(\mathbf{A}'_{\psi^A} + \hat{\mathbf{A}}_{\delta_F^A}\right)\delta_F^A \tag{14}$$

$$\frac{d\delta_F^S}{dt} = \mathbf{S}\delta_F^S \tag{15}$$

The forced-atmosphere error is governed by two terms in (14). The first is a local effect which damps errors along UA-convergent directions and amplifies them along UA-divergent directions. Suppose that the forced-atmosphere state ψ_F^A is close to the true solution ψ^A, so that δ_F^A is small and the second term in (14) can be ignored. Then, whenever the true solution visits regions of phase space where all directions are UA-convergent, the small error δ_F^A shrinks exponentially and the forced solution gets even closer to the true solution. We shall call such regions of phase space *binding regions*, since they tend to "bind" forced trajectories to the true solution.

The UA atmosphere model $\mathbf{A}_{\psi^A}\psi_A$ can be expressed in cylindrical coordinates as

$$\frac{dx}{dt} = -R^2 - ax \tag{16}$$

$$\frac{dR}{dt} = (x-c)R \tag{17}$$

$$\frac{d\theta}{dt} = bx \tag{18}$$

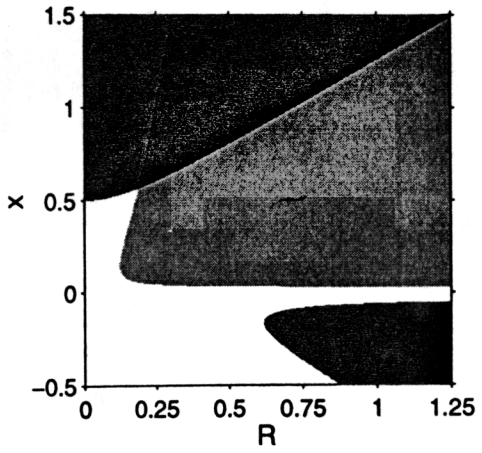

Fig. 6. Real parts of the three eigenvalues of the prototype-atmosphere Jacobian $\mathbf{A}'_{\psi^A}$. The bounding box of this figure sweeps out a cylindrical region of phase space which just contains the attractor of Fig. 1a. Shading indicates the number of eigenvalues with a positive real part: black=3, dark shading=2, light shading=1. White demarcates a "binding region" where all three eigenvalues have a negative real part.

where x is the same as in (1)–(3), $R = (y^2 + z^2)^{1/2}$ is the distance from the x-axis, and $\theta = \arctan(z/y)$ is an azimuthal angle from the positive y-axis. The evolution of (16)–(18) is independent of θ, so the vector field defined by $\mathbf{A}_{\psi^A}\psi_A$ is invariant under phase-space rotations about the x-axis. Thus the eigenvalues of the Jacobian $\mathbf{A}'_{\psi^A}$ are independent of θ; their real parts are plotted versus x and R in Fig. 6. The white area demarcates the binding region where all three eigenvalues have a negative real part, and all eigendirections are UA-convergent. Whenever ψ_A passes through this binding region, $\mathbf{A}'_{\psi^A}$ in (14) acts to reduce the magnitude of the forced error δ_F^A, effectively "binding" forced trajectories to the true solution. Outside the binding region, $\mathbf{A}'_{\psi^A}$ acts to amplify δ_F^A in one or more directions, driving forced trajectories away from the true solution.

The second term in (14) is quadratic in δ_F^A, and must be considered when δ_F^A is comparable to ψ_A in magnitude. The undamped UA model $\hat{\mathbf{A}}_{\psi^A}\psi^A$ takes the form

$$\frac{dx}{dt} = x^2 - r^2 \tag{19}$$

$$\frac{dr}{dt} = 0 \tag{20}$$

$$\frac{d\theta}{dt} = bx \tag{21}$$

where $r^2 = x^2 + y^2 + z^2$. Equation (20) implies that trajectories of $\hat{\mathbf{A}}_{\psi^A}\psi^A$ evolve on a sphere of radius r (Fig. 7). The equations (19)–(21) are invariant under $(x, t) \to (-x, -t)$, so time reversal corresponds to mirroring trajectory paths about the plane $x = 0$. The equations are also invariant under $(x, r, t) \to (kx, kr, k^{-1}t)$, where k is any constant, so larger spheres support faster trajectories. On each concentric sphere there are two fixed points $\psi^A_{\pm r} = (\pm r, 0, 0)$. Since x can never increase, ψ^A_r is a source while ψ^A_{-r} is a sink. In

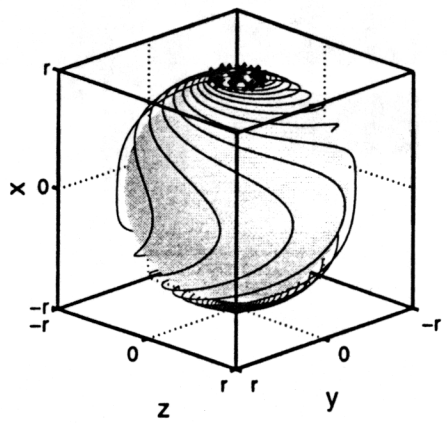

Fig. 7. Trajectories of $\hat{\mathbf{A}}_{\psi^A}\psi^A$ remain on a sphere of radius r centered about the origin; they spiral out from the source at $x = r$ and into the sink at $x = -r$. The trajectories shown (thin lines) emanate from a ring of initial conditions (crosses) about the x-axis near $x = r$.

short, the instantaneous effect of $\hat{\mathbf{A}}_{\delta_F^A}$ in (14) is to rotate δ_F^A in space, without changing its magnitude.

We can now easily explain the strange behavior of the forced model described in Section 3. Whenever the true solution approaches the binding region of Fig. 6, the linear term $\mathbf{A}'_{\psi^A}\delta_F^A$ in (14) acts to reduce δ_F^A. If the forced solution lies near the true solution so that $\|\delta_F^A\| \ll \|\psi^A\|$, the linear term dominates and the forced model locks to the true solution. As the true solution continues to evolve, it eventually enters a UA-divergent region where the forced error begins to grow exponentially. As δ_F^A grows, the nonlinear term $\hat{\mathbf{A}}_{\delta_F^A}\delta_F^A$ in (14) begins rotating the error vector. Only when the true solution reenters the binding region, and $\|\delta_F^A\|$ is small enough that nonlinearities are negligible, can the forced model again lock to the true solution.

Expanding one forced state about another gives an equation for the distance between two forced trajectories, identical in form to (14):

$$\frac{d\delta^A_{F(i),F(j)}}{dt} = \left(\mathbf{A}'_{\psi^A_{F(i)}} + \hat{\mathbf{A}}_{\delta^A_{F(i),F(j)}}\right)\delta^A_{F(i),F(j)} \qquad (22)$$

where $i \neq j$. Note that (22) reduces to (14) when one of the forced trajectories is taken to be the true solution. The true atmosphere ψ^A can be viewed as another forced trajectory, a very special one in which the ocean "forcing" is always exactly consistent with the atmospheric state. The binding region of Fig. 6, which tends to bind forced trajectories to the true solution, also tends to squeeze forced trajectories together independent of the state of the true solution. Since the forced model spends a good deal of time in the binding region (see Section 3), occasionally all forced trajectories get bound together as in year 66 of Fig. 3. When the true solution subsequently visits the binding region, the forced atmospheres lock to the true solution and synchronize with the ocean forcing. The newly-coherent forcing then induces atmospheric instabilities which drive the forced ensemble out of the binding region along with the true solution. Outside the binding region forced errors grow exponentially along UA-divergent directions, so that the forced atmospheres diverge from the true solution and once again become inconsistent with the ocean forcing.

This conceptual picture helps explain the strange "binding" and "locking" behavior of the forced ensemble in Fig. 3. It also explains why the inner portion of the forced ensemble is so poorly populated by the true solution in Fig. 5 and Table 2: the binding region reduces the spread of the forced solutions, hampering their ability to encompass the true solution. Thus it seems that the forced inconsistencies described in Section 3 stem from the lack of coherent air-sea interactions in the forced model. This causes forced trajectories to linger and converge in a "binding region" where their spread decreases independent of the state of the true solution. When the true solution finally enters the binding region, the forced ensemble can lock to the true solution and be pulled away from the binding region by consistent ocean forcing.

According to (15), the OMIP error δ_F^S evolves according to the constant, uncoupled ocean operator $\mathbf{S}$. Thus in the conceptual model, OMIP errors do not grow or shrink; they simply revolve in a p-q circle with constant frequency ω. Adding dissipation to the ocean model would cause OMIP perturbations to decay, no matter what the prescribed atmospheric forcing.

This section has shown that in forced models of the form (8), perturbations evolve according to *uncoupled* dynamics. If a subsystem is linear and dissipative in the absence of coupling, then forcing it with prescribed linear fluxes will cause perturbed trajectories to converge to the true solution. However, if a subsystem is nonlinear in the absence of coupling, then forcing it with prescribed fluxes can cause perturbed trajectories to converge to solutions inconsistent with the true coupled system.

5 Predictability in a forced model

Equation (22) indicates that as long as the forced atmospheres are close to the true solution, the spread and the error of the ensemble are related by similar local effects. Long after perturbation, however, errors become large and nonlinearities become important. Nevertheless, Fig. 3 indicates that forced trajectories continue to approach one another in the binding region, independent of the state of the true solution, so that the spread of the forced ensemble becomes a poor indicator of its instantaneous error. Such is the case in year 66 of Fig. 3b, where the forced ensemble spread decreases long before the ensemble attains skill by locking to the true solution.

Let $\langle\lambda\rangle$ denote the *ensemble mean* of a variable λ:

$$\langle\lambda\rangle \equiv \frac{1}{N}\sum_{j=1}^{N}\lambda_j \qquad (23)$$

where the sum is over the N ensemble members ψ_j. We define the *spread* of the coupled ensemble to be its standard

deviation:

$$\sigma_C \equiv \sqrt{\frac{N}{N-1}\left\langle \left\| \psi^A_{C(j)} - \langle \psi^A_C \rangle \right\|^2 \right\rangle} \tag{24}$$

The *error of the ensemble mean*, i.e. the distance between the ensemble mean and the true solution, is

$$\mu_C \equiv \left\| \langle \psi^A_C \rangle - \psi^A \right\| \tag{25}$$

The spread σ_F and error μ_F of the forced ensemble are similarly defined.

Fig. 8 presents scatterplots of μ vs. σ (with $N = 9$) for snapshots taken every five days during the first year after perturbation. Initially the ensemble members are tightly clustered about the true solution so that both σ and μ are small. As the ensembles disperse along the attractor of Fig. 1a, both the spread and the error increase. There are few cases with both small spread and large error. In a least-squares sense, the true solution seems to stay "inside" the ensemble, so that the ensemble mean is almost always as close to the true solution as it is to the ensemble members themselves. Thus σ is nearly an upper bound for μ during the first year. There are also few cases with large spread and small error in Fig. 8; in fact the points fall fairly close to the line $\mu = \sigma$. This is because the attractor of the prototype system has a rather "hollow" structure, so that its time-mean state lies in a region of phase space rarely visited by model trajectories. As the ensemble spread increases, μ grows because the ensemble mean moves inside the attractor shell where it rarely encounters the true solution.

Fig. 8b is very similar to Fig. 8a, except for an extended tail of very compact and accurate forced ensembles stretching toward the lower left of Fig. 8b. This extended tail can be explained using the concepts of Section 4. Soon after perturbation, the forced solutions are still close to the true solution. The spread of this compact ensemble is governed by the linear term in (14), so when the ensemble enters a binding region, both the spread and the error of the forced ensemble must decrease. Fig. 8a shows no such low-spread low-error tail, apparently because coupled feedbacks dominate over the binding term in the coupled model for small spreads. Thus at short leads the forced ensembles provide useful information about the true solution, because feedbacks have had little cumulative effect on the coupled system.

Fig. 9 is a scatterplot of μ vs. σ for snapshots taken every 100 days between years 10 and 50 after perturbation. At these longer leads the coupled ensemble has dispersed along the model attractor, so that σ_C and μ_C remain near their climatological values. The forced ensemble, on the other hand, exhibits more variability in its spread and error. Fig. 9b shows that long after perturbation, the spread of the forced ensemble is a poor indicator of the error of the ensemble mean. Forced ensembles with small spread can be quite inaccurate, while the most accurate forced ensembles do not always have the smallest spread. This is in contrast to the strong spread-skill relationship evident shortly after perturbation (Fig. 8). The forced model apparently alters the ensemble spread in a manner inconsistent with coupled dynamics, and unrelated to the ensemble skill. This highlights a possible danger in relating the spread of AMIP-type ensembles to the predictability of the climate system: *at long leads, reproducibility in a forced model does not necessarily imply skill, nor does skill necessarily imply reproducibility*, even in this case where both the model and its prescribed components are perfect.

The temporal inconsistency of the true solution and the forced ensemble, noted in Section 3.3, is evident in Fig. 9b. At each time, the standard deviation σ_F of the forced ensemble is the best linear unbiased estimate (in a least-squares sense) of the distance between an ensemble member and the ensemble mean. If at each time the true solution were drawn from the same distribution as the forced ensemble, the expectation for the error μ_F would simply be the ensemble standard deviation σ_F. In other words, if the true solution were consistent with the forced ensemble, the least-squares fit to the values of μ_F in Fig. 9b would be the line $\mu_F = \sigma_F$. This is clearly not the case in Fig. 9b; errors are larger than expected when the ensemble is compact, so that most snapshots lie well above the line $\mu_F = \sigma_F$. This indicates, as in Section 3.3, that the forced ensemble has too little temporal variance to be consistent with the true solution at long leads.

One might suppose that since the forced model has fewer degrees of freedom than the coupled model, forced trajectories should exhibit less spread than coupled trajectories. In other words, one might expect σ_F to always be less than σ_C. Fig. 10a shows that during the first year, σ_F can be a factor of two greater than σ_C. Thus *at short leads, where initial values still have influence, reproducibility is not necessarily greater in a forced model than in a coupled model.* At long leads (Fig. 10b), σ_F is a good lower bound for σ_C, but this is only because the two spreads are no longer related: σ_F can be large or small, while σ_C is always large.

This section has shown that the spread-skill relationship in a forced model can be quite different from that in a coupled model. At short leads, the forced ensemble can reduce its spread and error by locking to the true solution in a binding region. Despite this, forced trajectories are not generally more reproducible than coupled trajectories at short leads. At long leads, reproducibility of forced trajectories does not necessarily imply skill, even in the "perfect" model context examined here.

6 Discussion

Creating and testing a realistic coupled GCM is a formidable task, one which is simplified greatly by breaking the problem into pieces. It would be nice if each piece could be developed separately, in an environment where interaction values were simply prescribed from real-world data. Various parameters could be then be tuned so that each component looked most realistic in this forced environment. However, experience has shown that such separately-developed components are often incompatible upon coupling (Sausen and Lunkeit, 1990). In

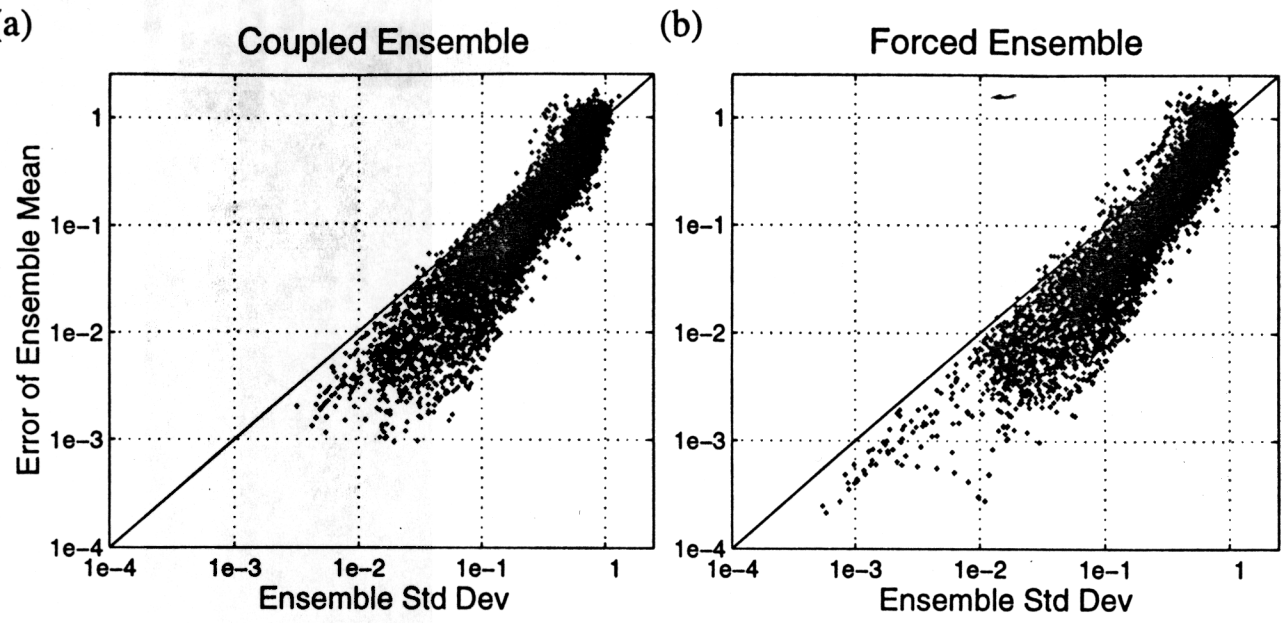

Fig. 8. Ensemble mean error μ vs. ensemble standard deviation σ, for (a) coupled atmospheres and (b) forced atmospheres. Points are plotted every five days during the first year after perturbation, for 100 different perturbation experiments begun at four-year intervals. Note the logarithmic scale. The line $\mu = \sigma$ is superposed for reference.

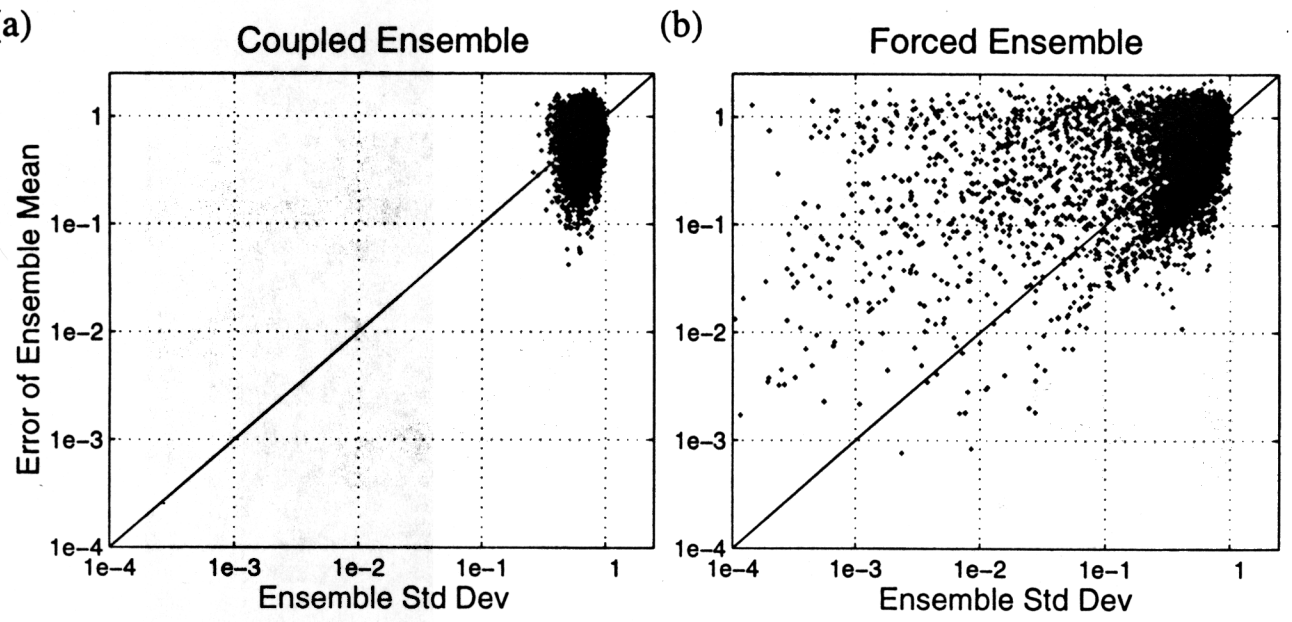

Fig. 9. As in Fig. 8, except points are plotted every 100 days between years 10 and 50 after perturbation.

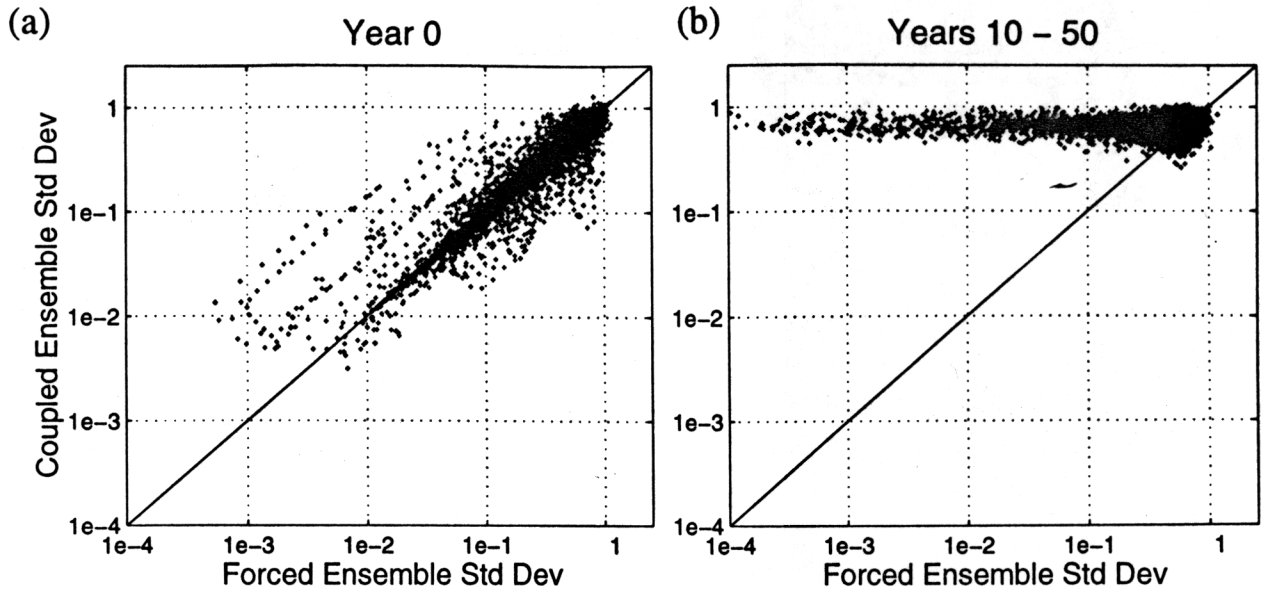

Fig. 10. Coupled ensemble standard deviation σ_C vs. forced ensemble standard deviation σ_F, for (a) the data of Fig. 8 and (b) the data of Fig. 9. If σ_F were a lower bound for σ_C, all points would lie above the diagonal line $\sigma_C = \sigma_F$.

a phenomenon known as *climate drift*, long-term means of dynamical quantities wander to unrealistic values. Climate drift is often ameliorated by adjusting interfacial fluxes, but this treats only certain symptoms of the coupled model, not the underlying problems in its components. In addition, such "flux adjustments" are worrisome for long-term climate prediction, since it is difficult to gauge their effects as the time-mean state changes (Neelin and Dijkstra, 1995).

The seeds of climate drift are planted early in the development of a coupled model, perhaps as its constituent parts are separately developed and tested in a forced-model context. This paper has shown that forcing a model with prescribed components can alter statistics of the model's climate and variability, yielding trajectories inconsistent with the true coupled solution. Tuning a model component in this environment may cause it to be ill-suited to its ultimate role in a fully-coupled system. For example, if the forced-model bias toward small x-values in Figs. 4 and 5 had been erroneously "corrected" by tuning the atmospheric model, the coupled system likely would have developed a "climate drift."

The root of forced-model inconsistency lies in the elimination of feedbacks vital for coupled instabilities. Removing these instabilities in the prototype model causes forced trajectories to linger and converge in a "binding region" of phase space, where perturbed forced trajectories coalesce and approach the true solution. As the forced ensemble spread decreases independent of the ensemble error, the ensemble becomes too compact to encompass the true solution. When the true solution visits the binding region, the forced atmospheres converge toward the true solution and synchronize with their ocean forcing. The consistent ocean forcing then induces atmospheric instabilities which mimic coupled instabilities, driving the forced atmospheres out of the binding region along with the true solution. Outside the binding region, the forced trajectories diverge from the true solution and once again become inconsistent with the ocean forcing. This cycle of error growth and decay differs from that in the coupled model. As a result, the forced ensemble evolves in a manner spatially and temporally inconsistent with both the true solution and the coupled ensemble. In addition, since the forced ensemble spread depends only on the phase-space convergence properties of the uncoupled atmosphere model, the reproducibility of forced trajectories is only loosely related to their skill at long leads.

Although the insights of Section 4 could apply to more complex forced models of the form (8), some caveats are in order. To facilitate a clear comparison with the true solution, the forced model in this study was presumed to have instantaneous, error-free forcing and perfect dynamics. Operational GCMs, however, may yet be too imperfect for forced-model inconsistencies to merit concern. The errors associated with sparse observations, coarse resolution, and approximate model equations might be much larger than those associated purely with prescription. Even in a low-order atmosphere model similar to the one in this study, Roebber et al. (1997) noted significant dynamical differences when the model was forced with monthly-mean SSTs instead of instantaneous SSTs.

The idealized AMIP system in this study had only three degrees of freedom, making it easy to find a "binding region" of phase space. In a binding region, all eigenvalues of the uncoupled, autonomous, tangent-linear forced subsystem are negative, so that nearby forced trajectories must converge. These regions might be difficult to find in a GCM with millions of degrees of freedom. However, confluences of flow in phase space are often found near quasi-stationary points

such as the ghosts of saddle-node bifurcations (Legras and Ghil, 1985). As trajectories tend to slow near such points, they can produce *regimes*, regions of the attractor preferred by the system (Mo and Ghil, 1987; Dymnikov et al., 1990, 1992; Marshall and Molteni, 1993; Dymnikov and Kazantsev, 1994; Dymnikov and Filatov, 1995). Thus the results of this study may be relevant more generally to systems which exhibit regime behavior. In systems without clear regime behavior, the inconsistencies associated with prescribing model subsystems could be more subtle than in the present case.

Often, prescribed forcing can help constrain an imperfect model to an accurate mean state, which may prove more essential for realistic variability than maintaining accurate coupled dynamics. In some cases, the model climatology itself is simply prescribed, and deviations from the climatology are predicted using an anomaly model linearized about a state of rest (e.g., Zebiak and Cane, 1987). This approach is conceptually useful and computationally economical, and has produced models with remarkable predictive skill. On the other hand, the lack of anomaly-climatology feedback in an anomaly model bears analogy with the lack of air-sea feedbacks in an AMIP model. Where the climate and variability are inextricably linked, an anomaly model may misrepresent the behavior of the fully-interacting system (Neelin and Dijkstra, 1995).

Despite these caveats, the results of this study could hold important implications for model development and validation. Dynamical inconsistencies have been shown to arise in AMIP GCM runs (see Introduction), and might also affect OMIP runs, two-tiered climate forecasts, and other contexts in which one or more model components are specified, including prescribed-cloud schemes (Ridout and Rosmond, 1996) and studies of troposphere-forced variability in the upper atmosphere (Hamilton, 1998). In the prototype system, accurate variability depends even more on the consistency of feedback dynamics than on the instantaneous accuracy of the prescribed forcing. These results could warrant additional attention to coupled feedbacks and their accurate simulation.

Appendix. The Prototype Coupled System

The prototype "atmosphere" model (1)–(3), in the absence of coupling to (4)–(5), is that of Lorenz (1984, 1990) and has been described in detail by Roebber (1995). This system was originally formulated to qualitatively describe midlatitude quasi-geostrophic flow. The variable x represents the mean meridional temperature gradient, or by thermal wind balance, the zonal-mean wind velocity. The variables y and z represent amplitudes of the cosine and sine phases of superposed eddies. The model time variable t has been rescaled as in Goswami et al. (1993) to slow the evolution by a factor c. The first column on the right of (1)–(3) represents eddy-mean flow interactions; terms linear in x, y, and z represent dissipation; the fourth column in (2)–(3) represents advection of the eddies by the zonal mean wind. The terms containing f and g in (1)–(2) represent zonally symmetric and asymmetric components of diabatic heating. In the absence of eddy-mean flow interactions, x would be driven toward f with e-folding time a^{-1}, and y would be driven toward g/c with e-folding time c^{-1}.

The prototype "ocean" model (4)–(5), in the absence of coupling to (1)–(3), is a simple harmonic oscillator. The oscillation frequency ω corresponds to a period of four years. The variables p and q could conceptually represent zonal asymmetries in SST, which interact with the model atmosphere's eddy field (y and z).

Using the notation of (6), the integration scheme is a second-order predictor-corrector of the form

$$\tilde{\psi}_{n+1} = \psi_n + \Delta t\,(\mathbf{C}_{\psi_n}\psi_n + \mathcal{B}_n) \tag{A1}$$

$$\tilde{\psi}_{n+2} = \tilde{\psi}_{n+1} + \Delta t\left(\mathbf{C}_{\tilde{\psi}_{n+1}}\tilde{\psi}_{n+1} + \mathcal{B}_{n+1}\right) \tag{A2}$$

$$\psi_{n+1} = \frac{\psi_n + \tilde{\psi}_{n+2}}{2} \tag{A3}$$

where $\Delta t = 0.025$ is a nondimensional time step corresponding to 6 model hours. The forced-atmosphere model consists of (1)–(3), with p and q prescribed from the true solution at every time step, including the trial steps $\tilde{\psi}$.

Parameter values for all integrations are as follows:

$$a = 0.125 \qquad b = 4 \qquad c = 0.5 \qquad \alpha = \beta = 0.1$$

$$f = 3.5 + \sin\left(\frac{\gamma t}{1\text{ year}}\right) \qquad g = 0.25$$

$$\gamma = \frac{1\text{ year}}{365.25\text{ days}} \times \frac{10\text{ days}}{1\text{ nondim unit}} \approx 0.0274\text{ year}$$

$$\omega = \frac{2\pi\gamma}{4\text{ years}} \qquad N = 9 \qquad \varepsilon = 0.01$$

For further details on the coupled system, see Goswami et al. (1993) and Krishnamurthy et al. (1993).

Acknowledgements. ATW was supported by a Graduate Research Fellowship from the National Science Foundation. The helpful comments of Olivier Pauluis, Kevin Hamilton, and R. Saravanan are gratefully acknowledged.

References

Anderson, J. L., A method for producing and evaluating probabilistic forecasts from ensemble model integrations, *J. Climate*, *9*, 1518–1530, 1996.

Barnett, T. P., Monte Carlo climate forecasting, *J. Climate*, *8*, 1005–1022, 1995.

Barsugli, J. J. and Battisti, D. S., The basic effects of atmosphere-ocean thermal coupling on midlatitude variability, *J. Atmos. Sci.*, *55*, 477–493, 1998.

Battisti, D. S. and Sarachik, E. S., Understanding and predicting ENSO, *Rev. Geophys., July 1995 Suppl.*, 1367–1376, 1995.

Bengtsson, L., Schlese, U., Roeckner, E., Latif, M., Barnett, T. P., and Graham, N., A two-tiered approach to long-range climate forecasting, *Science*, *261*, 1026–1029, 1993.

Bladé, I., The influence of midlatitude ocean-atmosphere coupling on the low-frequency variability of a GCM. Part I: No tropical SST forcing, *J. Climate*, *10*, 2087–2106, 1997.

Chen, W. Y. and Van den Dool, H. M., Atmospheric predictability of seasonal, annual, and decadal climate means and the role of the ENSO cycle: a model study, *J. Climate*, *10*, 1236–1254, 1997.

Dymnikov, V. P. and Filatov, A. N., On several problems of mathematical theory of climate, *Izv. Acad. Sci. USSR, Atmos. Oceanic Phys.*, *31*, 293–303, 1995.

Dymnikov, V. P. and Kazantsev, Y. V., On the structure of an attractor described by the equations for the barotropic atmosphere, *Izv. Acad. Sci. USSR, Atmos. Oceanic Phys.*, *29*, 557–571, 1994.

Dymnikov, V. P., Kazantsev, Y. V., and Kharin, V. V., Stability measures and lifetimes of atmospheric circulation regimes, *Izv. Acad. Sci. USSR, Atmos. Oceanic Phys.*, *26*, 253–259, 1990.

Dymnikov, V. P., Kazantsev, Y. V., and Kharin, V. V., Information entropy and local Lyapunov exponents of barotropic atmospheric circulation, *Izv. Acad. Sci. USSR, Atmos. Oceanic Phys.*, *28*, 425–432, 1992.

Gallimore, R. G., Simulated ocean-atmosphere interaction in the North Pacific from a GCM coupled to a constant-depth mixed layer, *J. Climate*, *8*, 1721–1737, 1995.

Gates, W. L., AMIP: the Atmospheric Model Intercomparison Project, *Bull. Amer. Meteor. Soc.*, *73*, 1962–1970, 1992.

Goswami, B. N., Selvarajan, S., and Krishnamurthy, V., Mechanisms of variability and predictability of the tropical coupled ocean-atmosphere system, *Proc. Indian Acad. Sci. (Earth Planet. Sci.)*, *102*, 49–72, 1993.

Graham, N. E., Barnett, T. P., Wilde, R., Ponater, M., and Schubert, S., On the roles of tropical and midlatitude SSTs in forcing interannual to interdecadal variability in the winter Northern Hemisphere circulation, *J. Climate*, *7*, 1416–1441, 1994.

Hamilton, K., Effects of an imposed quasi-biennial oscillation in a comprehensive troposphere-stratosphere-mesosphere general circulation model, *J. Atmos. Sci.*, *55*, 2393–2418, 1998.

Harzallah, A. and Sadourny, R., Internal versus SST-forced atmospheric variability as simulated by an atmospheric general circulation model, *J. Climate*, *8*, 474–495, 1995.

Kang, I.-S. and Lau, N.-C., Principal modes of atmospheric variability in model atmospheres with and without anomalous sea surface temperature forcing in the tropical Pacific, *J. Atmos. Sci.*, *43*, 2719–2735, 1986.

Krishnamurthy, V., Goswami, B. N., and Legnani, R., A conceptual model for the aperiodicity of interannual variability in the Tropics, *Geophys. Res. Lett.*, *20*, 435–438, 1993.

Kumar, A., Hoerling, M., Ji, M., Leetmaa, A., and Sardeshmukh, P., Assessing a GCM's suitability for making seasonal predictions, *J. Climate*, *9*, 115–129, 1996.

Latif, M., Biercamp, J., von Storch, H., McPhaden, M. J., and Kirk, E., Simulation of ENSO related surface wind anomalies with an atmospheric GCM forced by observed SST, *J. Climate*, *3*, 509–521, 1990.

Latif, M., Kleeman, R., and Eckert, C., Greenhouse warming, decadal variability, or El Niño? An attempt to understand the anomalous 1990s, *J. Climate*, *10*, 2221–2239, 1997.

Lau, N.-C., Modeling the seasonal dependence of the atmospheric response to observed El Niños in 1962-76, *Mon. Wea. Rev.*, *113*, 1970–1996, 1985.

Lau, N.-C. and Nath, M. J., A modeling study of the relative roles of tropical and extratropical SST anomalies in the variability of the global atmosphere-ocean system, *J. Climate*, *7*, 1184–1207, 1994.

Legras, B. and Ghil, M., Persistent anomalies, blocking and variations in atmospheric predictability, *J. Atmos. Sci.*, *42*, 433–471, 1985.

Livezey, R. E., Masutani, M., and Ji, M., SST-forced seasonal simulation and prediction skill for versions of the NCEP/MRF model, *Bull. Amer. Meteor. Soc.*, *77*, 507–517, 1996.

Lorenz, E. N., Irregularity: a fundamental property of the atmosphere, *Tellus*, *36A*, 98–110, 1984.

Lorenz, E. N., Can chaos and intransitivity lead to interannual variability?, *Tellus*, *42A*, 378–389, 1990.

Marshall, J. and Molteni, F., Toward a dynamical understanding of planetary-scale flow regimes, *J. Atmos. Sci.*, *50*, 1792–1818, 1993.

McCreary, Jr, J. P. and Anderson, D. L. T., An overview of coupled ocean-atmosphere models of El Niño and the Southern Oscillation, *J. Geophys. Res.*, *Feb. 1996 Suppl.*, 3125–3150, 1991.

Miller, A. J. and Roads, J. O., A simplified coupled model of extended-range predictability, *J. Climate*, *3*, 523–542, 1990.

Mo, K. C. and Ghil, M., Statistics and dynamics of persistent anomalies, *J. Atmos. Sci.*, *44*, 877–901, 1987.

Neelin, J. D. and Dijkstra, H. A., Ocean-atmosphere interaction and the tropical climatology. Part I: The dangers of flux correction, *J. Climate*, *8*, 1325–1342, 1995.

Philander, S. G. H., Ocean-atmosphere interactions in the Tropics: A review of recent theories and models, *J. Appl. Meteor.*, *31*, 938–945, 1992.

Press, W. H., Teukolsky, S. A., Vetterling, W. T., and Flannery, B. P., *FORTRAN: The Art of Scientific Computing*, Cambridge University Press, 2nd edn., 1992.

Ridout, J. A. and Rosmond, T. E., Global modeling of cloud radiative effects using ISCCP cloud data, *J. Climate*, *9*, 1479–1496, 1996.

Roebber, P. J., Climate variability in a low-order coupled atmosphere-ocean model, *Tellus*, *47A*, 473–494, 1995.

Roebber, P. J., Tsonis, A. A., and Elsner, J. B., Do climate simulations from models forced by averaged sea surface temperature represent actual dynamics?, *Nonlin. Proc. Geophys.*, *4*, 93–100, 1997.

Rowell, D. P., Folland, C. K., Maskell, K., and Ward, M. N., Variability of summer rainfall over tropical north Africa (1906-92): Observations and modeling, *Quart. J. Roy. Meteor. Soc.*, *121*, 669–704, 1995.

Saravanan, R., Atmospheric low-frequency variability and its relationship to midlatitude SST variability: Studies using the NCAR Climate System Model, *J. Climate*, *11*, 1386–1404, 1998.

Saravanan, R. and McWilliams, J. C., Stochasticity and spatial resonance in interdecadal climate fluctuations, *J. Climate*, *10*, 2299–2320, 1997.

Saravanan, R. and McWilliams, J. C., Advective ocean-atmosphere interaction: An analytical stochastic model with implications for decadal variability, *J. Climate*, *11*, 165–188, 1998.

Sausen, R. and Lunkeit, F., Some remarks on the cause of the climate drift of coupled ocean-atmosphere models, *Contrib. Atmos. Phys.*, *63*, 141–146, 1990.

Stern, W. and Miyakoda, K., Feasibility of seasonal forecasts inferred from multiple GCM simulations, *J. Climate*, *8*, 1071–1085, 1995.

Ward, N. M. and Navarra, A., Pattern analysis of SST-forced variability in ensemble GCM simulations: Examples over Europe and the tropical Pacific, *J. Climate*, *10*, 2210–2220, 1997.

Zebiak, S. E. and Cane, M. A., A model El Niño-Southern Oscillation, *Mon. Wea. Rev.*, *115*, 2262–2278, 1987.